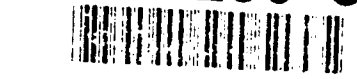

Technical Report ARAED-TR-92024

YIELD AND PLASTIC FLOW IN COMPOSITION B AND TNT

J. Pinto
D. A. Wiegand

January 1993

US ARMY
ARMAMENT MUNITIONS
& CHEMICAL COMMAND
ARMAMENT RDE CENTER

U.S. ARMY ARMAMENT RESEARCH, DEVELOPMENT AND ENGINEERING CENTER

Armament Engineering Directorate

Picatinny Arsenal, New Jersey

The views, opinions, and/or findings contained in this report are those of the authors(s) and should not be construed as an official Department of the Army position, policy, or decision, unless so designated by other documentation.

The citation in this report of the names of commercial firms or commercially available products or services does not constitute official endorsement by or approval of the U.S. Government.

Destroy this report when no longer needed by any method that will prevent disclosure of its contents or reconstruction of the document. Do not return to the originator.

REPORT DOCUMENTATION PAGE

Form Approved OMB No. 0704-0188

1. AGENCY USE ONLY (Leave blank)	2. REPORT DATE	3. REPORT TYPE AND DATES COVERED
	January 1993	

4. TITLE AND SUBTITLE

YIELD AND PLASTIC FLOW IN COMPOSITION B AND TNT

5. FUNDING NUMBERS

6. AUTHOR(S)

J. Pinto and D. A. Wiegand

7. PERFORMING ORGANIZATION NAME(S) AND ADDRESSES(S)

ARDEC, AED
Energetics and Warheads Div (SMCAR-AEE-WW)
Picatinny Arsenal, NJ 07806-5000

8. PERFORMING ORGANIZATION REPORT NUMBER

Technical Report
ARAED-TR-92024

9.SPONSORING/MONITORING AGENCY NAME(S) AND ADDRESS(S)

ARDEC, IMD
STINFO Branch (SMCAR-IMI-I)
Picatinny Arsenal, NJ 07806-5000

10. SPONSORING/MONITORING AGENCY REPORT NUMBER

11. SUPPLEMENTARY NOTES

12a. DISTRIBUTION/AVAILABILITY STATEMENT

Approved for public release; distribution is unlimited.

12b. DISTRIBUTION CODE

13. ABSTRACT (Maximum 200 words)

The yield strengths and elastic properties of trinitrotoluene (TNT) and a composite (Composition B) of TNT and cyclotrimethylene trinitramine (RDX) have been studied by confined triaxial compression (uniaxial strain) as a function of temperature and strain rate. The yield strength of Composition B decreases with increasing temperature and decreasing strain rate, while more limited results for TNT indicate that the yield strength of the TNT used in this investigation decreases slightly with increasing temperature and is insensitive to strain rate. The results for Composition B can be explained in terms of thermally activated dislocation motion over short range barriers while the results for TNT indicate that dislocation motion is controlled by (athermal) long range internal stress fields. The results further indicate that the yield strengths and so the magnitudes of the long range internal stress fields are about the same for TNT and Composition B close to the TNT melting temperature.

14. SUBJECT TERMS

Composition B, TNT, Triaxial stress, Yield strength, Young's modulus, Poisson's ratio, Friction, Dislocations, Thermal activation, Short range barriers, Internal stress fields

15. NUMBER OF PAGES
54

16. PRICE CODE

17. SECURITY CLASSIFICATION OF REPORT	18. SECURITY CLASSIFICATION OF THIS PAGE	19. SECURITY CLASSIFICATION OF ABSTRACT	20. LIMITATION OF ABSTRACT
UNCLASSIFIED	UNCLASSIFIED	UNCLASSIFIED	SAR

ACKNOWLEDGMENTS

The authors are indepted to S. Nicolaides for active participation in the planning stages for this work and for helpful discussions throughout, D. Georgevich and M. Mezger for assistance with data taking, and to M. Mezger and Y. Lanzerotti for helpful discussions. The authors wish to thank C. Ribaudo for material characterization, G. Ziegler for casting TNT and Comp B, J. Jenkins for the machining of samples, and F. Glanzel for radiographic work.

CONTENTS

	Page
Introduction	1
Background	2
Experimental	7
Results	9
Composition B	9
TNT	13
Summary of Experimental Results	15
Discussion	16
Temperature and Strain Rate Dependence of the Yield Strength of Composition B	16
Temperature and Strain Rate Dependence of the Yield Strength of TNT	21
Comparison of the Yield Strengths of Comp B and TNT	22
Summary and Conclusions	23
References	41
Distribution List	45

FIGURES

		Page
1	Experimental setup for triaxial loading under radial confinement	29
2	Radial stress versus axial stress for Comp B for the high strain rate conditions	30
3	Radial stress versus axial stress for TNT for the high strain rate conditions	31
4	Axial stress versus axial strain for Comp B for the high strain rate conditions	32
5	Axial stress versus axial strain for TNT for the high strain rate conditions	33
6	Typical axial stress and axial strain rate versus time for Comp B for the high strain (load) rate conditions	34
7	Maximum shear stress versus axial strain for Comp B for the high strain rate conditions	35
8	Yield strength versus temperature for Comp B for the high strain rate conditions	36
9	Yield strength versus temperature for Comp B for the low strain rate conditions	37
10	Maximum shear stress versus axial strain for TNT for the high strain rate conditions	38

Figures (continued)

		Page
11	Yield Strength versus temperature for TNT for both the low and high strain rate conditions	39
12	Apparent activation volume, V_τ, versus temperature calculated from the experimental results of figures 6 and 7	40

INTRODUCTION

This report is the second in a series dealing with the mechanical properties of trinitrotoluene (TNT) and a composite (Composition B) of TNT and cyclotrimethylene trinitramine (RDX). In the first report, the results of uniaxial compression studies of these materials as a function of temperature and strain rate are reported with particular attention being devoted to the uniaxial compressive fracture properties (ref 1). Under uniaxial stress conditions, these materials fail by brittle fracture for all conditions studied. However, if they are subjected to confined triaxial stress (uniaxial strain) conditions, fracture does not occur and failure occurs by yielding (ref 2). The results of confined triaxial loading of TNT and Composition B (Comp B) are reported. The yield strength as determined by this type of loading has been studied as a function of temperature and strain rate. The elastic properties were also studied and are given here for ambient conditions. The elastic properties as a function of temperature and strain rate will be reported in reference 3.

The studies reported were undertaken in part because very little information and understanding is available on the mechanical properties and mechanical failure of molecular organic polycrystalline solids. In addition, TNT and Comp B are important military explosives. Knowledge of the mechanical properties and, in particular, the conditions for failure are very important relative to the use of these materials. Mechanical failure is thought to play a critical role in ignition/initiation (refs 4 through 7). The conditions of stress and temperature experienced during cast cooling, handling, and in use such as projectile launch are of special importance. Therefore, studies were made for two strain rates: a quasi-static rate which is appropriate for cast cooling and some handling conditions, and a higher rate which is applicable to other conditions of handling and to weapons use such as artillery launch.

TNT and Comp B were prepared by casting from the melt (ref 2). Comp B is made by adding particulate RDX and wax to TNT and contains 39.5% TNT, 59.5 % RDX, and 1% wax. During the casting, process and cooling defects such as dislocations, cracks, porosity, and larger cavities are often introduced. These defects are important because they are thought to play critical roles in ignition and initiation. For example, dislocations may play a role in impact initiation of explosives (ref 7), and all of these defects may play roles in premature ignition during artillery launch (ref 8). Some of these defects are caused by stresses during cast cooling, e.g., thermal stresses, and mechanical properties are needed for these conditions of temperature and strain rate for modeling so as to be able to predict cooling conditions which will not result in defect generation. Therefore, measurements were made at the low quasi-static strain rate. In addition, measurements are needed at higher strain rates for modeling to predict failure conditions and possible ignition conditions with defects during use, e.g., during projectile launch and as a result of impact and shock. For these reasons measurements were made at the higher strain rate.

Complete stress-versus-stress and stress-versus-strain curves have been recorded as a function of temperature and strain rate with most attention being devoted to the yield strength. The goal is to develop a basic understanding of these materials which will enable predictions of failure conditions and, in particular, failure conditions leading to ignition or initiation. However, at no time during the course of these studies was any evidence of decomposition or ignition observed.

BACKGROUND

The uniaxial compressive strength of these brittle materials is dependent on flaws such as cracks or voids where stress concentrations can develop and failure takes place by crack propagation (ref 1). This type of brittle failure is not observed if fracture is hindered by triaxial confinement (ref 2) (fig. 1) and experimental techniques have been used to determine the mechanical properties of brittle materials under this type of triaxial loading (ref 9). By using this triaxial loading, it is possible to determine the yield strength in addition to the elastic constants. This type of triaxial loading with radial confinement (uniaxial strain) has been used to study Comp B, TNT, and other similar materials over a range of temperatures and strain rates (refs 2, 10, 11). It has also been used to simulate the loading conditions encountered by explosives during artillery launch and is the same type of loading used in various activators to study and determine the setback sensitivities of explosives (refs 12 through 14). The same general experimental techniques are used in this work. Another type of triaxial loading has been used to study polymeric energetic materials (propellants) and is sometimes referred to as biaxial loading (refs 15 and 16).

The stress-strain relationships can be written as:

$$\varepsilon_i = \sum_{i,j} S_{ij}\sigma_j \qquad (1)$$

where ε_i are the strains, σ_j are the stresses, and S_{ij} are the elastic compliances. For triaxial loading normal to the surface in three orthogonal directions taken as tne x, y, and z axes (fig. 1) and for an isotropic material, equations 1 reduce to:

$$\varepsilon_x = S_{11}\sigma_x + S_{12}\sigma_y + S_{12}\sigma_z \qquad (2a)$$

$$\varepsilon_y = S_{12}\sigma_x + S_{11}\sigma_y + S_{12}\sigma_z \qquad (2b)$$

$$\varepsilon_z = S_{12}\sigma_x + S_{12}\sigma_y + S_{11}\sigma_z \qquad (2c)$$

where it can be shown that Young's modulus, E, and Poisson's ratio, v, are:

$$E = \frac{1}{S_{11}} \tag{3a}$$

$$v = \frac{-S_{12}}{S_{11}} \tag{3b}$$

The sign convention taken here is that v is a positive number. For the triaxial experimental procedure used here, a cylindrically shaped specimen is enclosed in a close fitting, thick-walled steel cylinder and compressed along the x axis as shown in figure 1. A tight fit between the specimen and the steel cylinder is obtained by increasing the temperature a few degrees until a hoop strain is observed on the outer wall of the steel tube. This occurs because the sample has a higher coefficient of thermal expansion than the steel. Since the cylinder tube is much stiffer than the test specimen, the strains in the specimen in the y and z directions are negligible. Also, from cylindrical symmetry

$$\sigma_x = \sigma_y = \sigma_r \tag{4}$$

Using this identity and $\varepsilon_y = \varepsilon_z = 0$, equation 5 is obtained from either equation 2a or 2b.

$$\sigma_r = \frac{v}{1-v}\sigma_a = m\sigma_a \tag{5}$$

where $\sigma_a = \sigma_x$. This equation shows that the slope, m, of the radial stress versus axial stress curve in the elastic region is determined by Poisson's ratio (figs. 2 and 3). Solving for v in terms of this slope m gives

$$v = \frac{m}{1+m} \tag{6}$$

Furthermore, if equations 3a, 3b, 4, and 5 are substituted into equation 2c and this solved forYoung's modulus, we obtain

$$E = \frac{\sigma_a}{\varepsilon_a}\left(1 - \frac{2v^2}{1-v}\right) \tag{7}$$

where $\varepsilon_a = \varepsilon_x$. After obtaining v from the slope of the σ_r versus σ_a curve, Young's modulus can be obtained from the slope of the axial (x direction) stress-versus-strain curve (figs. 4 and 5). The shear modulus, G, and the bulk modulus, K, can then be calculated using the measured values of E and v.

It is necessary to point out that in this report the term elastic is used rather loosely to refer to the initial linear portions of stress-versus-strain and stress-versus-stress curves before yield. The elastic constants refer to these linear regions and may not be equal to the elastic constants determined in other ways, e.g., by methods using much smaller deformations and much higher rates such as ultrasonic techniques.

These equations apply to a material which is in an elastic state of stress. Under continued action of an applied axial stress, the material will eventually undergo a transition from an elastic to a plastic state. This transition is characterized by yield. Various criteria can be used to determine yield (refs 17 through 19). The von Mises criterion, which is based on yield occurring when the strain energy of distortion reaches a critical value, can be stated as

$$Y_{vm} = \frac{1}{\sqrt{2}} \sqrt{(\sigma_x-\sigma_y)^2+(\sigma_x-\sigma_z)^2+(\sigma_y-\sigma_z)^2} \qquad (8)$$

where Y_{vm} is the von Mises yield strength. Y_{vm} can be determined from a uniaxial experiment, i.e., when $\sigma_y = \sigma_z = 0$, $Y_{vm} = \sigma_x$ at yield. The same criterion is obtained by determining yield by the condition that the octahedral shearing stress reaches a critical value (refs 17 and 18). Another criterion for yield is based on the maximum shearing stress reaching a critical value (refs 17 through 19). This is often referred to as the Tresca criterion (ref 19) and can be stated as

$$Y_t = |\sigma_x - \sigma_y| \qquad (9)$$

where $|\sigma_x - \sigma_y|$ is greater than $|\sigma_y - \sigma_z|$ and $|\sigma_z - \sigma_x|$. Y_t can also be obtained by a uniaxial test where $Y_t = \sigma_x$ at yield when $\sigma_y = \sigma_z = 0$. These two yield criteria (eqs 8 and 9) do not give identical yield strengths for all conditions of loading (ref 19). However, for the triaxial conditions used in this work, i.e., $\sigma_y = \sigma_z = \sigma_r$, we obtain from both equations 8 and 9

$$Y_t = Y_{vm} = Y = \pm(\sigma_a - \sigma_r) \qquad (10)$$

where the $\pm$ sign indicates that both $\sigma_a > \sigma_r$ and $\sigma_a < \sigma_r$ are possible solutions to equations 8 and 9. The yield strength is taken as a positive number. Therefore, both the Tresca and the von Mises yield criteria give identical yield strengths in this case. As pointed out immediately above, Y is the yield strength as determined in a uniaxial experiment. However, for Comp B and TNT, the yield strength as obtained from equation 10 is more than twice the uniaxial compressive fracture strength (refs 1 and 2). In the uniaxial case, fracture occurs before yield and so the yield strength cannot be obtained from a uniaxial test. Additional discussion of this point is given in reference 1.

These considerations indicate that for the experimental conditions used here the radial stress versus axial stress curve will have a break, with the initial or elastic region being determined by equation 5 and the yield or plastic region being determined by equation 10 (figs. 2 and 3). Poisson's ratio is obtained from the slope in the elastic region (eqs 5 and 6) and the yield strength, Y, is obtained from the intercept of the yield line (eq 10) with the σ_a axis.

Equations 5 and 10 have been obtained for the ideal case of negligible friction between the cylindrical surface of the explosive sample and the cylindrical inner wall of the confining cylinder (fig. 1)[1] By the methods developed in reference 2 and to be considered in greater detail separately (ref 20), these equations become

$$\sigma_r \, me^{-4fm} \quad \sigma_a = m'\sigma_a \tag{11}$$

$$Y = \sigma_a - \sigma_r e^{4f} \tag{12}$$

where f is the coefficient of friction between the explosive and the steel and the + sign has been taken for the case of increasing σ_a (eq 10).[2] In obtaining equations 11 and 12, it is assumed that the frictional forces are small, i.e., f«1. This condition has been found to be obeyed for the results presented. f is obtained from the measured angle β as shown in figures 2 and 3 from the relationship (ref 20)

$$\tan \beta = e^{-4f} \tag{13}$$

---

[1] Many of the effects which are attributed to friction in this report can also be attributed to work hardening or to a combination of friction and work hardening. Detailed studies to determine the relative importance of friction and work hardening are now in progress.

[2] In the appendix of reference 2 it is erroneously stated that 1 = 2r rather than 1 = 2d = 4r. Because of this, some of the equations of this appendix contain an error of a factor of two. l, r, and d are the length, radius, and diameter of the sample.

When friction is present, the relationships between the measured quantities σ_a, σ_r, and ε_a are modified (refs 2 and 20). In particular, the relationship between σ_a and σ_r as measured is modified because σ_a and σ_r are actually functions of the distance from the end of the sample where σ_a is applied and measured while σ_r is measured at the midpoint of the sample as shown by the position of the strain gauges in figure 1. As indicated by equation 11, the slope of the σ_r versus σ_a curve in the elastic (initial) region on loading is reduced relative to the value without friction (eq 5). The slope in the yield region during loading with friction (eq 12) is also reduced relative to the value without friction (eq 10). Yield occurs when σ_a and σ_r satisfy both equations 11 and 12 with increasing σ_a and equation 12 is followed for further increases of σ_a if flow occurs without work hardening. The coefficient of friction, f, is obtained from the measured angle β by the use of equation 13. Poisson's ratio can then be obtained from the measured slope, m', in the elastic region by the use of equations 5, 6, and 11. The yield strength is obtained as in the case without friction by the intercept on the σ_a axis (eq 12).

Without friction, the axial stress and strain are independent of the distance from the end of the sample, and Young's modulus, E, can be obtained from the slope of the σ_a versus ε_a loading curve by using equation 7. Because the axial stress is a function of this distance when friction is present, the axial strain is also a function of this distance (refs 2 and 20). The measured quantity is, however, the average axial strain as determined by the displacement of the two anvils (fig. 1). The net effect of friction in the elastic region is to reduce the average axial strain relative to the value without friction for a given applied axial stress (ref 20). The slope of the measured σ_a versus ε_a curve is increased relative to the value without friction, and equation 7 can no longer be used to obtain the modulus E. The following equation gives the desired relationship between E and the measured quantities σ_a and ε_a when friction must be considered (ref 20):

$$E = \frac{\sigma_a}{\varepsilon_a}\left[1 - \frac{2\nu^2}{1-\nu}\right]\left[\frac{1 - e^{-4mf}}{4mf}\right] \qquad (14)$$

The maximum shearing stress τ is given by

$$\tau = \frac{\sigma_a - \sigma_r}{2} \qquad (15)$$

and in the elastic region for the case without friction this becomes

$$\tau = \frac{\sigma_u (1\text{-}m)}{2} \tag{16}$$

by the use of equation 5. Therefore, the maximum shearing stress increases linearly with σ_a (and ε_a). In the yield regions, the maximum shearing stress is

$$\tau = \pm \frac{Y}{2} \tag{17}$$

if flow occurs without work hardening. This result is obtained by using equation 10. Therefore the maximum shearing stress is constant in the yield region without work hardening as σ_a (and ε_a) increase. Equations 15 through 17 apply for the case without friction. When friction is present, σ_a and σ_r are functions of the distance from the end of the sample, and τ must be calculated using σ_a and σ_r for the same position (refs 2 and 20). In terms of the measured quantities σ_a and σ_r, the maximum shearing stress is given by

$$\tau = \frac{\sigma_a e^{-4fm} - \sigma_r}{2} \tag{18}$$

in the elastic region and by

$$\tau = \frac{\sigma_a - \sigma_r e^{4f}}{2} \tag{19}$$

in the yield region (ref 20).

EXPERIMENTAL

The loading apparatus and the data handling processes are described in reference 1 as are the sample preparation procedures. Additional details are given in reference 2. The samples were all in the form of right circular cylinders of lengths approximately 1.5 inches and diameters close to 0.752 inch. The sample lengths were uniform and parallel to within ± 0.001 inch and the diameters were uniform to within ± 0.005 inch. A range of sample diameters were obtained, but they were all less than 0.750 inch which is the inner diameter of the steel confining cylinder of figure 1.

The experimental arrangement for studying the mechanical properties under radial confinement is shown in figure 1. The confining test cylinders are made of hardened steel and have an inner diameter of 0.7520 ± 0.0001 inch. The inner cylindrical walls have a ground 8G surface finish. The anvils were also made of hardened steel, have diameters of 0.7502 ± 0.0001 inch, and have ground 8G finishes. The tolerances given for the inner diameter of the cylinders and the outer diameter of the anvils are conservative. Therefore, the radial clearance between the cylinder and the anvil is approximately 0.001 or less. SR-4 strain gages were glued to the outside of the test cylinder to measure the hoop strain. This hoop strain is related to the internal radial stress exerted by the test specimen on the steel cylinder by the equation

$$\sigma_r = \frac{E'(b^2 - a^2)}{2a^2}\varepsilon_r = 6.64 \text{ X } 10^7\varepsilon_r \qquad (20)$$

where a and b are the inner and outer radii of the test cylinder, E′ is the elastic modulus of the cylinder material, ε_r is the hoop strain, and σ_a is the radial stress exerted by the specimen on the cylinder. E′ was measured for the steel cylinders used in these studies and found to be 3.01 X 10^7 psi.

A tight fit must exist between the test specimen and the walls of the test cylinder. Since it was desired to measure these properties as a function of temperature, test specimens were machined to a variety of diameters near 0.752 inch, the inner diameter of the steel confining cylinder. Then, by calculating a dimensional change for a specified temperature change, a specimen of the proper diameter could be chosen, placed in the test cylinder, and heated to the desired temperature in the conditioning box (ref 1). Since the thermal coefficients of expansion of Comp B and TNT are greater than that of steel, this procedure enabled the specimen to come into contact with the walls of the steel test cylinder. This contact and a tight fit between the specimen and the steel was detected as a hoop strain by the strain gauges attached to the outer wall of the steel cylinder (fig. 1).

In order to minimize binding and friction inside the test cell, the entire specimen was coated with a thin film of graphite powder before being placed in the cell. The effects of friction on the measure quantities were discussed above. Thermocouples were attached to various locations on the test cylinder, on the anvils, and on the metal parts in contact with the test fixture. The test fixture was at this point resting on the bottom crosshead. The experiment was carried out when all of the thermocouples indicated that thermal equilibrium had been attained. When thermal equilibrium was reached at the desired temperature, the test fixture was brought into contact with the upper heated crosshead, a small prestress of approximately 50 psi was applied to the specimen, and a load-versus-time profile programmed into the computer was applied

to the specimen. It was necessary to use the servo-hydraulic system in load control for this work because a maximum load (stress) and not a maximum displacement (strain) as used in reference 1 had to be stipulated. Two loading rate conditions were used: a constant low loading (axial stress) rate of 625 psi/s and a high loading rate which was not constant and was determined by the fastest response of the system. The low loading rate resulted in a constant strain rate in the elastic region of approximately 10^{-3} s^{-1} for Comp B and a somewhat greater value for TNT and a variable strain rate in the yield regions because of curvature of the axial stress-versus-strain curves (figs. 4 and 5).

For the high rate loading condition, a high strain rate which varied with time (fig. 6) was obtained. In this figure, typical curves of axial stress and axial strain rate versus time are given for Comp B for the high loading rate condition. The strain rate increased to a maximum value of approximately 8.0 s^{-1} at small times and then decreased with increasing time, reached a value of about 0.2 s^{-1} at about 20 ms, and a value of about 0.1 s^{-1} at about 40 ms (not shown) which is the end of the increasing stress part of the experiment. The noise in the strain rate versus time data of figure 6 is due mostly to noise in the linear variable differential transformer (LVDT) although a part of the noise is also due to analogue-to-digital and digital-to-analogue conversions which are necessary to capture, store, and analyze the raw data from the LVDT. An inspection of figure 2 for Comp B indicates that the elastic (initial) range extends from zero axial stress to an axial stress of about 22,000 psi. The data of figure 6 indicate that the strain rate varies over a range of about 8 s^{-1} to 4 s^{-1} for this range of axial stress, neglecting the initial acceleration. The strain rate then decreases as the axial stress increases into the yield region. However, the results indicate that the yield strength and so the latter part of the radial versus axial stress curve is insensitive to strain rate (fig. 7). High strain rate as referred to the data presented in this report refers to the strain rate conditions of figure 6. Low strain rate refers to the conditions of low constant load (stress) rate as stated above.

RESULTS

Composition B

Samples of Comp B obtained from the split mold casts and from the smaller cardboard tube casts (refs 1 and 2) were studied in triaxial loading using the confined cylinder geometry illustrated in figure 1. The applied axial stress, σ_a, and the average axial strain, ε_a, as determined by the displacement of the anvils, were measured and the radial stress, σ_r, was calculated as indicated above. A typical curve of σ_r versus σ_a at 35°C for the high rate conditions is given in figure 2. Similar curves were

obtained at the low strain rate. The elastic (initial) region at low σ_a and the yield (plastic) region at higher σ_a on loading (increasing σ_a) are indicated by the straight lines. These straight lines have been fitted to the curve by eye, and there is some subjectivity inherent in the process although considerable effort has been made to minimize subjective effects. The angle β, in general, has been found to be less than 45 deg so that frictional effects should be considered (eq 13). The coefficient of friction, f, can be obtained by the use of equation 13 and the measured value of β, and the value of m can be obtained from equation 11 and the measured value of m′ using either a graphical or an approximate analytical procedure (ref 20). Poisson's ratio, ν, can then be calculated from equation 6, and the yield strength, Y, is obtained by the intercept method as illustrated in figure 2.

A typical curve of σ_a versus ε_a is given in figure 4 also showing the linear elastic (initial) region at low and increasing σ_a. A straight line has been fitted by eye to the data of figure 4 in the initial region and the modulus E (Young's modulus) was obtained from the slope of this line using equation 14. A straight line can also be fitted by eye to the yield portion of the loading curve of figure 4. From the data of figures 2 and 4, the following are obtained: Y = 7500 psi, E = 0.61 x 10^6 psi, ν = 0.36, β = 40 deg, and f = 0.044. These values compare favorably with the average values given for the high strain rate in the table. The data in this table also indicate that the yield strength, Young's modulus, the shear modulus, the bulk modulus, and probably Poisson's ratio are higher at the higher strain rate. The values of the moduli and Poisson's ratio in the table for the low strain rate were taken at 35°C from least squares straight lines fitted to the data as a function of temperature. This was done because of the scatter in the data and because a sufficient number of samples were not measured in the vicinity of 35°C to give meaningful averages. The value of the yield strength at the low strain rate obtained in the same manner is the same as the average value given in the table.

Clark and Schmitt (ref 11), using the same experimental technique, obtained the following average values for measurements on six samples at 30°C at a high strain rate comparable to that used here: Y = 7950 ± 670 psi, E = (1.97 ± 1.00) x 10^6 psi, ν = 0.29 ± 0.04, and β = 38 deg ± 6 deg. They did not correct for frictional effects, but the magnitude of the angle β indicates that these corrections are necessary. In addition, the intersection technique was used to obtain Y, i.e., Y was calculated as the difference between σ_a and σ_r at the point of intersection of the straight lines for the elastic (initial) and yield regions (fig. 2) instead of using the intercept on the σ_a axis (eq 12). The use of the intersection technique and not correcting for friction leads to higher values of Y (ref 20). Not correcting for friction also leads to smaller values for ν

and a higher value for E. With these considerations in mind, the values of Y and ν which Clark and Schmitt report are in approximate agreement with the values given in the table as obtained in this work. However, the value of E reported by these investigators is much larger than the value found in this work, and this large difference cannot be attributed to frictional effects. Large values for E were also found by Clark and Schmitt in uniaxial studies (refs 10 and 11), and larger values of E are reported by Costain and Motto (ref 21). This discrepancy is discussed further in reference 1. By using strain gauged samples and uniaxial compression under both static and the high strain rate conditions, Clark and Schmitt found values of Poisson's ratio which are somewhat larger than the values which they report for high rate triaxial compression. They also made triaxial measurements on Comp B which were apparently vacuum cast and obtained somewhat larger values for the yield strength (ref 11).

Some of the results of uniaxial compressive studies of Comp B at 23°C and reported in reference 1 are given in the table for comparison purposes. The values of Young's modulus at the high and low strain rates obtained by triaxial compression are in agreement with the values obtained by uniaxial compression. Since the modulus decreases with increasing temperature, this agreement is better than indicated in the table because of the different temperatures for the triaxial and uniaxial results (refs 1 and 2). In addition, measurements in uniaxial compression on strain gauged samples gave values of Poisson's ratio which are close to the values given in the table for triaxial compression. It is important to note that the compressive fracture strength is significantly less than the yield strength at both strain rates. This result indicates that crack growth to fracture during triaxial compression is prevented by the radial confinement not present in the uniaxial case, and that yield and macroscopic dislocation motion does not take place for uniaxial loading because fracture occurs at a significantly lower stress.

The maximum shearing stress at the midpoint of the cylindrical sample as given by equations 18 and 19 for the elastic (initial) and yield regions respectively is plotted versus the axial strain in figure 7. Aside from the deviations in the immediate vicinity of the origin which are due to the sample establishing firm contact with the steel cylinder on initial loading, the data of figure 7 indicate an elastic (initial) region followed by a yield (plastic) region without work hardening. A straight line with the predicted slope (eqs 11 and 18) has been drawn through the data points in the elastic (initial) region and agrees well with the average slope of the experimental points. In the yield region, the maximum shearing stress is constant and equal to Y/2. The data of figure 7 indicate a value of Y of about 7200 psi which is close to but somewhat less than the value given above and obtained from figure 2 by the intercept method. The decrease of the maximum shearing stress and so Y at the largest values of axial strain may be due to strain rate effects (fig. 8) because the strain rate decreases appreciably in this

region as indicated in figure 9. The results presented in figures 2, 4, and 7 indicate that in the so-called yield region Comp B deforms at a constant shear or flow stress (yield stress) for these conditions of loading.

Samples were also investigated as a function of temperature between approximately 20°C and 75°C at the two strain rates and the yield strength, Young's modulus and Poisson's ratio were determined as a function of these parameters using the methods indicated above. The shear and bulk modulus were calculated using the measured values of Young's modulus and Poisson's ratio. However, only the temperature and rate dependencies of the yield strength will be considered here. The elastic properties will be treated separately, but in summary, Young's modulus decreases with increasing temperature much as reported in reference 1 while Poisson's ratio increases slightly with increasing temperature, the shear modulus decreases with increasing temperature, and the bulk modulus is insensitive to temperature (ref 3). The yield strength as a function of temperature is given for the low strain rate in figure 9 and for the high strain rate in figure 8. At both strain rates the yield strength decreases approximately linearly with increasing temperature, and the yield strength is larger for the higher strain rate, but the difference decreases with increasing temperature. In the temperature range of 75°C to 80°C or close to the melting temperature of TNT (81°C), the yield strengths at the two strain rates become equal. The data indicate that the yield strength is rather insensitive to strain rate since a strain rate increase of approximately a factor of 4×10^3 only results in an increase of about 30% in the yield strength at 30°C. Clark and Schmitt report yield strengths over a much more limited temperature range, and the results suggest a decrease with increasing temperature (ref 11). From the straight line for the high strain rate of figure 7, the yield strength decreases from about 8400 psi at 20°C to about 3500 psi at 70°C. This decrease of the yield strength of over a factor of two over a limited portion of the temperature range of military interest indicates that the conditions for safe launch of an artillery projectile at 20°C may not be safe at 70°C.

The compressive strength also decreases with increasing temperature and increases with increasing strain rate (refs 1 and 2). However, the compressive strength is somewhat more strain rate dependent than the yield strength, and there is no evidence that the compressive strengths at the low and high strain rates approach each other as the temperature approaches the melting temperature of TNT as is the case for the yield strengths (refs 1 and 2). Differences between the temperature and strain rate dependencies of the compressive strength and the yield strength are to be expected, because the compressive strength is determined by crack properties while the yield strength is related to dislocation properties.

TNT

Samples of TNT were also studied in triaxial compression and a typical curve of radial stress versus axial stress at 35°C and the high strain rate is given in figure 3. A comparison of figure 3 with figure 2 will reveal that these results for TNT are very similar to those for Comp B except that yield occurs at significantly lower values of the radial and axial stresses, and that Y is significantly lower. The angle β is 41 deg for these data for TNT and so friction should be considered in the data analysis as for Comp B. The axial stress versus axial strain data is plotted for the same sample (fig. 5). In this case, a comparison with figure 4 for Comp B will reveal that there are differences. After the initial elastic region, there is a region of roughly constant slope as for Comp B, but then the slope increases appreciably for TNT with further increases of axial stress. This latter increase was observed for TNT at all temperatures investigated at both strain rates but was not observed for Comp B at 35°C at the high strain rate (fig. 4). It was observed for Comp B at the low strain rate and at the high strain rate only at the highest temperatures. The details of the stress-versus-strain and stress-versus-stress curves will be considered separately (ref 20). In addition, the maximum axial strain for TNT is greater than for Comp B for the same maximum axial stress.

The data of figures 3 and 5 were analyzed in the same way as the data for Comp B, and the following results were obtained: $Y = 2750$ psi, $E = 0.31 \times 10^6$ psi, $\nu = 0.40$, $\beta = 41$ deg, and $f = 0.035$. Average values for TNT at the high strain rate are given in the table and indicate that the yield strength and the modulus are low and that Poisson's ratio is average for this sample. The angle β is slightly higher and so the friction coefficient, f, is slightly lower than the values for the sample of Comp B of figures 2 and 4. Clark and Schmitt (ref 11) have made compressive triaxial measurements of the same type at a high rate which is approximately the same as the rate used in this investigation. Their results for the yield strength for TNT indicate considerably higher values than the results presented here. Although they did not correct for friction and used the intersection technique to determine Y as discussed above for Comp B, the difference between their results and our results (almost a factor of two) cannot be completely attributed to the differences in data analysis. It seems necessary to conclude at this time that there are important differences between the samples used by Clark and Schmitt and those used in this investigation. This point is considered further below. The dependency of the mechanical properties on composition will be considered separately in some detail (ref 23).

The values of Poisson's ratio obtained by Clark and Schmitt for triaxial loading at the high strain rate are slightly lower, and the values of Young's modulus are considerably higher than the values found in this investigation and given in the table.

As noted for the case of Comp B, these investigators did not correct for friction although the magnitudes of the reported angles β indicate that this correction is desirable. The slightly lower values of Poisson's ratio reported by Clark and Schmitt may be due to this effect but the much larger values of Young's modulus cannot be due to frictional effects. They also obtained by uniaxial compression of strain gauged samples at high strain rate values of Poisson's ratio which are slightly lower and values of Young's modulus which are considerably higher than the values in the table. Costain and Motto also report significantly larger values of Young's modulus at a strain rate close to the lower strain rate used here (ref 21). This matter is discussed further in reference 1.

An inspection of the table will reveal that the yield strength of TNT at 35°C and the high strain rate is considerably less than the value for Comp B for the same conditions of measurement and that Young's modulus and the shear modulus of TNT are also a good bit less than the values for Comp B. The bulk modulus of Comp B may also be somewhat higher than the value for TNT, and the value of Poisson's ratio may be slightly higher for TNT. The larger yield strength for Comp B indicates the effect of the addition of 59.5% RDX and 1% wax to TNT on the stress necessary for macroscopic dislocation motion. The larger modulus of Comp B indicates that the modulus of RDX is greater than the modulus of TNT, and the smaller value of Poisson's ratio is indicative of the same property of RDX, i.e., that RDX is stiffer than TNT and so deforms less than TNT in general under any given elastic loading conditions.

In the table, some of the results of uniaxial compressive studies at 23°C and reported in reference 1 are given. The value of Young's modulus for TNT at the high strain rate obtained by triaxial compression is in agreement with the value obtained from uniaxial compression studies. As for Comp B, this agreement between the moduli as obtained from uniaxial and triaxial loading is better than indicated because of the difference in temperature for the two types of experiments as given in the table. It is also interesting to note that the compressive fracture strength of TNT is significantly lower than the yield strength as is the case for Comp B. Only one sample of TNT was measured at the low strain rate and at the lower end of the temperature range of investigation for triaxial compression. The results for this sample gave values of the yield strength and Young's modulus which are anomalously high and are not included in the table.

The maximum shear strength, τ, corrected for the effects of friction has been calculated for the sample of TNT of figures 3 and 5 in the same manner as for Comp B discussed above and is plotted as a function of axial strain in figure 10. The results are similar to the results for Comp B in that an elastic (initial) region is found for low values of axial strain, and a plateau follows indicating a constant flow stress. The points in the immediate vicinity of the origin do not lie on the elastic (initial) line

because the sample has not yet made completely firm contact with the steel cylinder. A straight line with the predicted slope (eqs 11 and 18) has been drawn in through the calculated points. From the plateau region, an approximate value of $\tau = Y/2$ of 1270; psi is obtained and so a value of Y = 2540 psi. This value is somewhat lower but close to the value obtained from figure 3 by the intercept method.

Very limited triaxial measurements were made for TNT as a function of temperature and strain rate. The available yield strength results at the low and the high strain rates are presented in figure 11 and indicate that the yield strength of TNT at the high strain rate is much less sensitive to temperature than is the yield strength of Comp B as given in figure 7. Because the scatter in the available data is so great, especially for the low rate data, very little can be concluded about the strain rate dependence other than that it is small. Clearly, additional measurements are necessary to resolve this matter further. The small temperature dependence, however, suggests that the mechanism controlling the temperature dependence in TNT may be different than the controlling mechanism for Comp B. Clark and Schmitt (ref 11) give values of the yield strength for TNT over the same temperature range as that of figure 11 at a high strain rate, but their data indicate a larger fractional decrease of Y with increasing temperature. These investigators also report considerably larger yield strengths for TNT than found in this investigation.

Summary of Experimental Results

A summary of the triaxial results at 35°C and a summary of some of the uniaxial results at 23°C from reference 1 are given in the table. The results indicate that the yield strength, the compressive fracture strength, and Young's modulus for Comp B are larger at the higher strain rate. The results further indicate that the compressive fracture strength and Young's modulus of TNT are larger at the higher rate, but the yield strength results are inconclusive as to the rate dependence (fig. 11). Young's moduli as determined from triaxial data are in agreement with the values obtained from uniaxial studies. The yield strengths and the compressive fracture strengths are both significantly larger for Comp B than for TNT, and Young's moduli are larger for Comp B, but the Poisson's ratios are probably larger for TNT. The latter results indicate that RDX is stiffer than TNT and so deforms less under elastic loading.

The yield strength of Comp B is rate dependent at 34°C, but the rate dependence decreases with increasing temperature so that the yield strengths at the two rates are about equal at the melting temperature of TNT. The yield strength of TNT is much less temperature dependent than the yield strength of Comp B, but the results for the rate dependence for TNT are inconclusive except that it is small. For both materials, Y decreases with increasing temperature and for Comp B, Y increases with increasing strain rate for temperatures below about 70°C.

DISCUSSION

In this section the temperature and strain rate dependencies of the yield strengths of Comp B and TNT are discussed separately and then compared.

Temperature and Strain Rate Dependence of the Yield Strength of Composition B

Because the RDX particles are embedded in the TNT matrix of Comp B, macroscopic yield and flow of Comp B cannot in general occur without yield and flow in the TNT of Comp B unless this TNT is capable of sustaining the relatively larger elastic strains that would be associated with plastic strains of the RDX particles. The yield and flow properties of TNT presented indicate that this is not the case. Therefore, unless the yield and flow properties of the TNT in the Comp B used in this study are significantly different from the yield and flow properties of the TNT used in this work, it can be concluded that the yield and flow of this Comp B necessarily involves the yield and flow of the TNT in this Comp B. From the results presented, it is not possible to determine if yield (or fracture) has occurred in the RDX particles of Comp B for the conditions of loading used in this study.

A review has been given recently of mechanisms which have been proposed to explain the strain rate dependence of the yield strength for a variety of conditions (ref 24). The temperature dependence of the yield strength of Comp B indicates a thermally activated process (refs 24 and 25). In this case, the average dislocation velocity is given by the relationship

$$v = sve^{\frac{-\Delta G}{kT_K}} = v_o e^{\frac{-\Delta G}{kT_K}} \tag{21}$$

where ΔG is the change in the Gibbs free energy (activation free energy), v is the frequency of vibration of the dislocation, and s is the distance moved in a successful jump (ref 24). Alternately, the preexponential term in equation 21 may be taken as v_o, the maximum shear wave velocity in the crystal (refs 24 and 25). The plastic shear strain rate is given by

$$\dot{\gamma} = \dot{\gamma}_o e^{\frac{-\Delta G}{kT_K}} \tag{22}$$

where

$$\dot{\gamma}_o = svb\rho_m = v_o b\rho_m \tag{23}$$

b is the Burger's vector, and ρ_m is the density of mobile dislocations (refs 24 and 25). The activation energy ΔG is, in general, a function of the shear stress, τ, and the absolute temperature, T_K (ref 25). Following others (refs 24, 26, and 27), it is assumed that ΔG is a linear function of the effective stress τ^* such that

$$\Delta G = \Delta G_o - \tau^* V_\tau \tag{24}$$

where V_τ is defined by

$$V_\tau \equiv -\left[\frac{\partial(\Delta G)}{\partial \tau^*}\right]_T = b\Delta a' \tag{25}$$

V_τ is sometimes called the activation volume (ref 24). As pointed out by Li, this activation volume should not be confused with the thermodynamic activation volume which is the partial derivative of ΔG with respect to pressure (ref 25). Here, V_τ will be referred to as the apparent activation volume and in the notation of Kocks, Argon, and Ashby (ref 28), this can be expressed in terms of an apparent activation area, $\Delta a'$ as given in equation 25. $\Delta a'$ is close to but not equal to the area swept out by a dislocation in a thermally activated jump. Equation 22 may then be rewritten as

$$\ln\frac{\dot{\gamma}}{\dot{\gamma}_o} = -\left[\frac{\Delta G_0 - \tau^* V_\tau}{kT_K}\right] \tag{26}$$

If the effective stress τ^* is the difference between the applied stress τ and an effective internal stress τ_i due to long range internal stress fields, i.e.,

$$\tau^* = \tau - \tau_i \tag{27}$$

then equation 26 may be rearranged to give

$$\tau = \tau_i + \frac{\Delta G_0}{V_\tau} - \frac{kT_K}{V_\tau}\ln\frac{\dot{\gamma}_0}{\dot{\gamma}} \tag{28}$$

The plastic strain rate (eqs 22, 24, and 27) will be negligible until τ reaches a critical value which may be taken as the shear stress at yield or Y/2. Therefore,

$$Y = 2\left[\tau_i + \frac{\Delta G_0}{V_\tau} - \frac{kT_K}{V_\tau}\ln\frac{\dot{\gamma}_0}{\dot{\gamma}}\right] \tag{29}$$

From equations 22, 25, and 26, V_τ is given by

$$V_\tau = kT_K\left[\frac{\partial \ln\frac{\dot{\gamma}}{\dot{\gamma}_0}}{\partial\tau^*}\right]_T \tag{30}$$

This equation for V_τ is independent of the assumed form for ΔG as given by equation 24. Since only two strain rates are available, the differential of equation 30 is approximated by finite differences so that this equation becomes

$$V_\tau = kT_K\left[\frac{\Delta \ln\frac{\dot{\gamma}}{\dot{\gamma}_0}}{\Delta\tau^*}\right]_T = \left[\frac{2kT_K\Delta(\ln\dot{\varepsilon})}{\Delta Y}\right]_T \tag{31}$$

where $\dot{\gamma}_0$ is assumed to be independent of τ and $\dot{\gamma}/\dot{\gamma}_0$ has been equated to $\dot{\varepsilon}/\dot{\varepsilon}_o$. $\dot{\gamma}_o$ (eq 23) should be independent of stress unless the density of mobile dislocations at yield changes with stress. While this cannot be ruled out, it will be assumed that this is not the case. V_τ has been obtained from equation 31 using the low and high strain rates and ΔY as obtained from the straight lines of figures 7 and 9, i.e.,

$$\Delta Y = 11{,}800 - 34T_K \tag{32}$$

V_τ and $1/V_\tau$ are plotted versus temperature in figure 12. An inspection of the expression for $1/V_\tau$ obtained from equations 31 and 32 will reveal why $1/V_\tau$ decreases approximately linearly with increasing temperature for the limited temperature range of this work as shown in figure 12. The change in the numerator of this expression is much greater than the change in the denominator for the extremes of temperature change of interest. Therefore, T_K in the denominator can be replaced by an average value without having a strong effect on the temperature dependence of $1/V_\tau$.

When the linear relationship between T_K/V_τ and the temperature obtained from equations 31 and 32 and the approximately linear relationship between $1/V_\tau$ and the temperature obtained from equation 31 as discussed immediately above or from figure 12 are inserted into equation 29, the following is obtained

$$Y = 2\tau_i + \frac{\left(\frac{\Delta G_o}{kT_{K\,avg}} - \ln\frac{\dot{\varepsilon}_o}{\dot{\varepsilon}}\right)(11{,}800 - 34\,T_K)}{\ln\frac{\dot{\varepsilon}_H}{\dot{\varepsilon}_L}} \qquad (33)$$

where the substitution $\dot{\gamma}_o/\dot{\gamma} = \dot{\varepsilon}_o/\dot{\varepsilon}$ has been made. For reasonable values of the quantities inside the first brackets, the difference is positive and the difference given by the second brackets is always positive since ΔY of equation 32 is always positive (fig. 8). The temperature and strain rate dependencies of Y as given by equation 33 are the same as the observed dependencies (figs. 8 and 9). Therefore, equation 33 predicts that Y should decrease linearly with increasing temperature at constant strain rate, and that Y should increase with increasing strain rate at constant temperature as observed. In addition, equation 33 predicts that the slope of the straight line for Y versus temperature should increase with increasing strain rate as observed. It is possible to interpret the temperature and strain rate dependencies of the yield strength of Comp B in terms of thermally activated dislocation motion over short range barriers by assuming a linear relationship between the activation energy and the effective stress (eq 24) and by assuming that $\dot{\gamma}_o$ (and $\dot{\varepsilon}_o$) is independent of τ. A somewhat similar explanation has been given by Campbell and Ferguson to account for the yield properties of mild steel (ref 29).

Equation 33 can be broken up into a temperature independent part and a part that is linearly dependent on temperature. Since Y has been found empirically to be described by an equation which is also in part temperature independent and a part which is linearly dependent on temperature (figs. 8 and 9), the empirical equation for Y may be equated to equation 33, and the resultant broken up into two equations. One equation arises because of the temperature independent terms, and the other equation comes from the coefficients of T_K. When this is done, the following two equations are obtained:

$$2\,\tau_i = 3.34 \times 10^{23}\,\Delta G_o - 9.72 \times 10^3 - 1.34 \times 10^3 \ln \dot{\varepsilon}_o = 24{,}900 \qquad (34)$$

$$9.64 \times 10^{20}\,\Delta G_o - 3.84 \times 10^3 \ln \dot{\varepsilon}_o = 90.8 \qquad (35)$$

The experimental value of $\dot{\varepsilon}$ for the low strain rate has been used in obtaining equations 34 and 35. Independent equations using the two strain rates of figures 8

and 9 are not obtained because the difference ΔY has already been used in obtaining the apparent activation volume V_τ from equation 31. Two relationships between the three unknown quantities τ_i, ΔG_o, and $\dot{\varepsilon}_o$ are given in equations 34 and 35. Estimates of τ_i and ΔG_o may be obtained by making an estimate of $\dot{\varepsilon}_o$. Since $\dot{\varepsilon}_o$ enters only through logarithmic terms, the values for τ_i and ΔG_o obtained in this way are not strongly dependent on the estimated value of $\dot{\varepsilon}_o$. This latter quantity has been estimated by using a relationship which is similar to that of equation 23, i.e.,

$$\dot{\varepsilon}_o = v_o' b\rho \qquad (36)$$

where v_o' is the longitudinal elastic wave velocity. This velocity was obtained from the measured value of Young's modulus, E (table 1) and the known density of Comp B. If b is taken as 10^{-7} cm and ρ_m as 10^7 cm^{-2}, a value of $\dot{\varepsilon}_o$ of 1.55×10^5 s^{-1} results. Substitution of this value of $\dot{\varepsilon}_o$ into equation 35 gives a value for ΔG_o of 1.42×10^{-19} joules (0.89 ev), and substitution of these values of $\dot{\varepsilon}_o$ and ΔG_o into equation 34 yields a value for τ_i of 1640 psi. The minimum value for $Y = 2\tau_i$ for region II of Rosenfield and Hahn (ref 30) and Campbell and Ferguson (ref 29) is 3280 psi. An inspection of figures 8 and 9 will reveal that only a few of the lowest values of Y at the highest temperatures are very close to this minimum value for Y. As pointed out, ΔG_o and τ_i are very insensitive to $\dot{\varepsilon}_o$. For example, a decrease of $\dot{\varepsilon}_o$ by two orders of magnitude results in a decrease of ΔG_o by only 14% and a decrease of τ_i by only 15%.

It is of interest to consider the possible role of the RDX in Comp B in forming obstacles to dislocation motion in the TNT of Comp B. The RDX particle size in Comp B varies from approximately 5×10^{-3} to 10^{-1} cm (ref 31). The cross-sectional area of the RDX particles varies from approximately 2.5×10^{-5} to 10^{-2} cm^2. If b is taken as of the order of 10^{-7} cm, then $\Delta a'$ can be obtained from equation 25 and the calculated values of V_τ given in figure 12. $\Delta a'$ therefore varies from about 0.6×10^{-14} to 5×10^{-14} cm^2. Since $\Delta a'$ is of the order of magnitude of the area swept out during an activated dislocation jump (ref 28), it can be concluded that the RDX particles are much too large to be the obstacles to dislocation motion of concern in the TNT of Comp B. However, RDX is also soluble in TNT and the solubility in the vicinity of 80°C is about 5% (ref 32). This temperature is close to the freezing temperature of Comp B (TNT). If RDX remains in solid solution in molecular form and is uniformly distributed in the solid TNT matrix, the spacing between molecules is of the order of 16×10^{-8} cm. Therefore, the area associated with an RDX molecule which a dislocation must sweep out in overcoming the RDX molecule as an obstacle is of the order of 2.5×10^{-14} cm^2. This area is of the same order of magnitude as the apparent activation area, $\Delta a'$, estimated above. It is possible that the obstacles to dislocation motion in the TNT of Comp B are

molecules of RDX or small aggregates of RDX molecules. It has been pointed out, however, that to obtain a significant temperature dependence of the yield strength due to dislocation-particle interactions it is necessary for the dislocations to shear the particles so as to increase the particle-matrix interface area (ref 33). For this to be the case, the RDX must be in the form of small clusters of at least two molecules per cluster. This question is also discussed by Brown and Ham (ref 34). The increase of $\Delta a'$ with increasing temperature could then be attributed to the clustering of RDX molecules and/or the growth of clusters of molecules with increasing temperature with an associated increase in the area swept out by dislocations in overcoming obstacles because of a decreasing density of obstacles. This clustering of RDX molecules gives a contribution to the activation entropy which decreases with increasing temperature. This cannot be the case, and an analysis of the data indicate that the activation entropy increases significantly with increasing temperature. It appears that small clusters of RDX molecules cannot be the obstacles to dislocation motion. This conclusion, however, is based on dislocations overcoming the RDX as obstacles by glide. Brown and Ham have considered the climb of an edge dislocation to bypass an idealized cubic particle and have arrived at an expression for the flow stress which varies with temperature and strain rate in the same manner as equation 29 if the cube decreases in size with increasing temperature in the appropriated manner (ref 35). If the particles are clusters of RDX molecules and if the particles decrease in size with increasing temperature by RDX molecules escaping into solid solution in the TNT, then the activation entropy will increase with increasing temperature as observed. At least qualitatively, it is possible to explain the observations in terms of thermally activated climb of edge dislocations over clusters of RDX molecules. Details of this and other processes including thermodynamic considerations will be considered separately (ref 36). The effects of various types of obstacles to dislocation motion is considered in reference 37.

Temperature and Strain Rate Dependence of the Yield Strength of TNT

Because of the very limited yield strength data for TNT as a function of temperature and because of scatter in the data, especially for the low strain rate, all discussion of the results for TNT must be taken as extremely tentative. With these limitations in mind, the very small temperature dependence of the yield strength at the high strain rate (fig. 11) suggests that dislocation motion is rate controlled by long range internal stresses in this case, i.e., by the athermal stress component, τ_i, of equation 27. Within the scatter in the data for the low strain rate (fig. 11), the results further suggest that the yield strength is also not very strain rate dependent. This lack of strain rate sensitivity supports the hypothesis that yield is determined by long range internal stresses. The long range internal stress fields have been discussed in some detail by Li (ref 25) and by Chen, Gilman, and Head (ref 37).

The athermal stress is generally attributed to dislocations and can be given by a relationship of the type

$$\tau_i = \alpha G b \sqrt{\rho_f + \rho_m} \qquad (37)$$

where α is a geometrical factor somewhat less than unity, G is the shear modulus, ρ_f is the density of fixed dislocations, and ρ_m is the density of mobile dislocations (refs 38 through 41). Young's modulus and Poisson's ratio were measured as a function of temperature for the TNT samples of figure 11 and the shear modulus calculated (ref 3). While the scatter in the data is too great to give an explicit temperature dependence for the shear modulus, the results indicate a small temperature dependence and so are not in disagreement with figure 11 and equation 37.

As noted in the results section, Clark and Schmitt have reported yield strengths of TNT which are significantly greater than the values found in this work (ref 11). In addition, the temperature dependence of the yield strength given by these investigators is significantly greater than the temperature dependence found in the present study. These results suggest that the yield properties of the TNT samples used by Clark and Schmitt were not determined solely by long range internal stress fields as they apparently are for the samples used in this investigation, but were also dependent on thermal activation over barriers due to short range stress fields associated with obstacles not present in the samples used in this study. Studies of the yield strength of samples of the type used in the present study at lower temperatures and/or higher strain rates may very well reveal that thermal activation over barriers due to short range stress fields is also important in these samples (refs 29 and 39).

Comparison of the Yield Strengths of Comp B and TNT

From the straight line of figure 11, Y for TNT varies from about 3400 psi at 20°C to about 2900 psi at 60°C. Therefore, τ_i = Y/2 varies from about 1700 psi to 1450 psi for the same temperature range. These values of τ_i are very close to the value of 1640 psi obtained for Comp B. It is also interesting to note that an extrapolation of the straight line of figure 11 for TNT to higher temperatures suggests that the yield strengths of TNT and Comp B (fig. 7) are very close as the temperature approaches the melting temperature of TNT. It is, therefore, tempting to conclude that the τ_i for Comp B is due to the long range stress fields in the TNT of Comp B because the dislocation densities in TNT and in the TNT in Comp B are not too different (eq 37). It is further very tempting to conclude that the obstacles to dislocation motion in Comp B which must be overcome by thermal excitation are associated with the RDX in the TNT matrix as already discussed for Comp B. There are, however, some difficulties with this general interpretation. While the TNT and the Comp B used in these studies were

obtained by cooling from the melt in approximately the same manner (ref 2), the presence of RDX and wax in Comp B might reasonably be expected to influence the dislocation densities and the internal strain fields in the TNT of Comp B. For example, a mismatch of the thermal expansion coefficients of TNT and RDX could cause dislocation generation during cooling from the melt. The RDX particles could also be the cause of long range strain fields because of misfit and elastic and thermal anisotropy. In addition, it is well known that the solidification properties of TNT are strongly influenced by the presence of other materials (ref 42). Very small additions of hexanitrostilbene to TNT very significantly reduce the grain size of TNT (ref 42). The grain size of the TNT of Comp B has been observed to be much smaller than the grain size of TNT alone for some conditions of preparation.[3] For these reasons the approximate equality in magnitudes of the long range internal stress fields for the Comp B and TNT used in these studies may be coincidental. Direct measurements of dislocation densities and structures are desirable.

SUMMARY AND CONCLUSIONS

The yield strengths and elastic constants of Comp B and TNT have been obtained as a function of temperature at two strain rates by radially confined triaxial compression (uniaxial strain). For this purpose the cylindrical explosive samples were placed in snug fitting steel confining cylinders of inner diameter equal to the diameter of the explosive samples and compressed axially. This geometrical arrangement was used to simulate the stress conditions which the explosive in a projectile experiences due to acceleration (and deceleration) during artillery launch. In addition, the same geometrical arrangement is used in various activators which are used to study the setback ignition/initiation sensitivity of explosives. Analysis of the data indicate that it is necessary to consider the effects of friction between the explosive sample and the inner cylindrical walls of the steel confining cylinder to obtain values for the yield strength and the elastic constants. Only the yield strength is reported and discussed here. The elastic property data will be reported separately (ref 3).

The yield strength of Comp B decreases with increasing temperature and decreasing strain rate for temperatures between 20°C and 75°C and two strain rates of approximately 10^{-3} s^{-1} and 4 s^{-1}. For the higher strain rate, yield occurs in a few milliseconds, and this corresponds to the time frame of artillery launch. The decrease of the yield strength at the higher strain rate in the temperature range of military interest is significant relative to the safe use of this explosive.

[3]Private communication with S. Morrow.

The rate and temperature dependencies of the yield strength of Comp B have been interpreted in terms of thermally activated dislocation motion over short range barriers for most of the temperature range considered. The results can be explained by a constant preexponential factor and an activation energy for this thermal activation which decreases linearly with increasing applied stress and is dependent on temperature through a temperature dependent apparent activation volume (or apparent activation area). The apparent activation volume increases with increasing temperature. The analysis also includes an athermal stress component and values for this athermal stress, the zero applied stress activation energy, and the preexponential factor are obtained. Dislocation motion and yield should be rate limited by the athermal stresses only close to the maximum temperatures investigated which are close to the melting temperature of TNT.

Much more limited results for TNT indicate that the yield strength for this explosive decreases somewhat with increasing temperature between 20°C and 60°C and is insensitive to strain rate for the two strain rates given above. As for Comp B, yield occurs in a few milliseconds at the high strain rate, but the decrease of the yield strength over the temperature range of military interest is not significant relative to the safe use of this explosive for the TNT used in these experiments. However, others have reported larger values for the yield strength of TNT and a greater decrease of yield strength with increasing temperature. Therefore, the yield properties of TNT are dependent on source and/or processing conditions.

The rate and temperature dependencies of the yield strength of the TNT used in this investigation can be interpreted in terms of athermal long range internal stress fields which resist dislocation motion. These internal stress fields are due to dislocation and/or other imperfections, and the temperature dependence of the yield strength is not inconsistent with the temperature dependence of the shear modulus.

Over most of the temperature range of this investigation, the yield strength of Comp B is greater than the yield strength of TNT. However, the results indicate that the yield strengths of these two explosives are about the same near the melting temperature of TNT (81°C). While the rate controlling mechanisms for dislocation motion are different for the two materials over most of the temperature range investigated, the results indicate that dislocation motion and yield is controlled by long range internal stress fields near the melting temperature of TNT in both materials. In addition, the magnitudes of the internal stress fields are close, suggesting that the dislocation densities (and/or densities of other imperfections) are not too far apart in the two materials. It can be inferred from this that dislocation motion and yield in Comp B occurs primarily in the TNT of this composite if the dislocation densities in the TNT in Comp B and in TNT alone are within a factor of two. Measurements of dislocation densities are necessary to further resolve this matter.

Additional measurements are desirable for Comp B at lower temperatures and at several strain rates or by differential techniques such as the change of strain rate and change of temperature tests to confirm the interpretation given to the yield strength results. Additional measurements are necessary for the whole range of temperatures and strain rates or changes of temperature and strain rate in order to confirm (or reject) the very tentative interpretation given to the yield properties of TNT. It is also desirable to cover the whole temperature range of military interest for both Comp B and TNT. Measurements of TNT with controlled impurities or additives are also desirable in order to understand the differences between the results presented here and the results of others. In addition, measurements of dislocation densities and structures for Comp B and TNT are highly desirable and will aid in the interpretation and understanding of the yield properties of these materials. And finally, studies of the yield phenomena of both materials as a function of impurities or additives can lead to significantly stronger, higher yield strength materials.

Table. Yield and fracture strengths and modulus properties* of Comp B and TNT at low and high strain rate

	RATE	COMP. B	TNT
TRIAXIAL: (T = 35°C)			
Y YIELD STRENGTH (PSI)	LOW	5600 ± 980	
	HIGH	7420 ± 1050	3350 ± 290
E YOUNG'S MODULUS ($\times 10^6$ PSI)	LOW	0.38	
	HIGH	0.54 ± 0.07	0.37 ± 0.06
ν POISSON'S RATIO	LOW	0.33	
	HIGH	0.36 ± 0.02	0.39 ± 0.02
G SHEAR MODULUS ($\times 10^6$ PSI)	LOW	0.15	
	HIGH	0.20 ± 0.03	0.13 ± 0.02
K BULK MODULUS ($\times 10^6$ PSI)	LOW	0.38	
	HIGH	0.63 ± 0.08	0.58 ± 0.07
β (°)	LOW	42.6 ± 0.2	
	HIGH	40.0 ± 1.5	40.3 ± 1.0
UNIAXIAL: (T = 23°C)			
σ COMPRESSIVE STRENGTH (PSI)	LOW	1680	960
	HIGH	3260 ± 150	1850 ± 180
E YOUNG'S MODULUS ($\times 10^6$ PSI)	LOW	0.36	0.25
	HIGH	0.60 ± 0.02	0.45 ± 0.07

*Determined from the slopes of the linear regions of the stress-versus-strain and stress-versus-stress curves below yield.

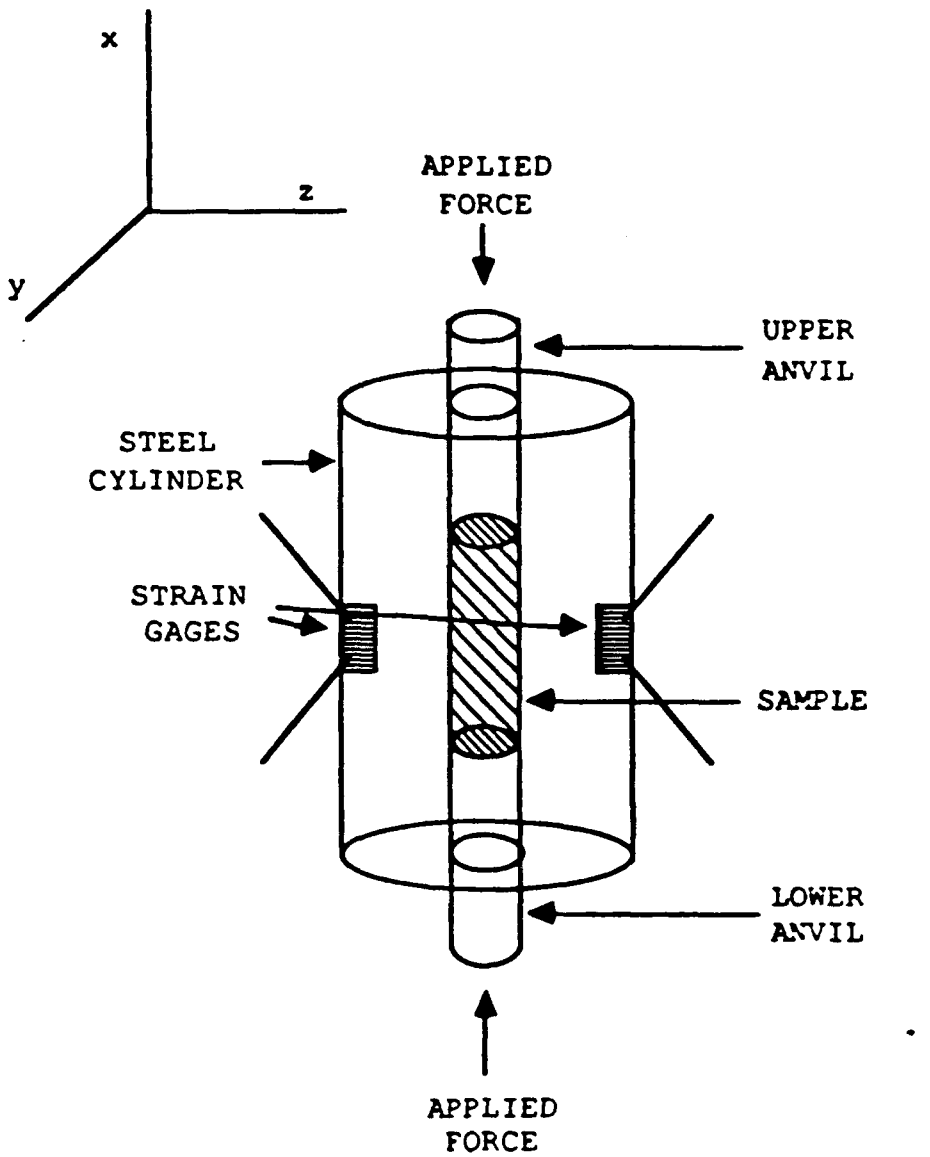

Figure 1. Experimental setup for triaxial loading under radial confinement

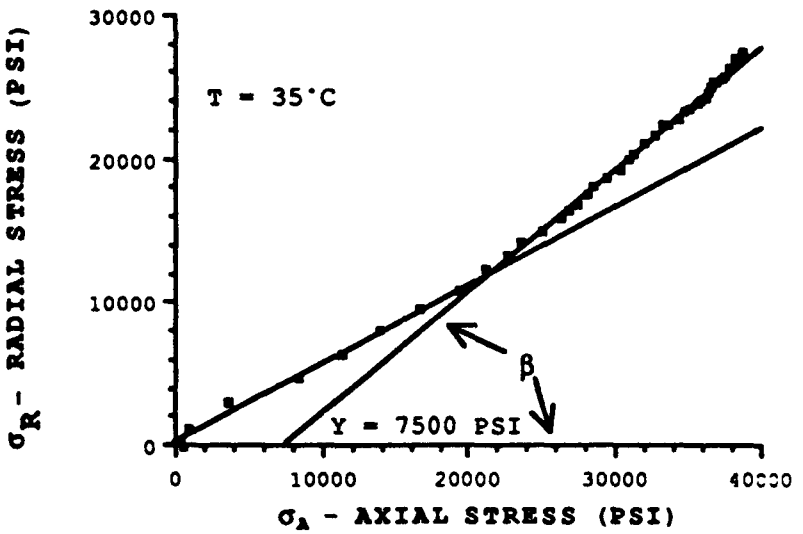

NOTE: Straight lines have been drawn through the elastic (initial) and yield parts of the loading curve as discussed in the text.

Figure 2. Radial stress versus axial stress for Comp B for the high strain rate conditions

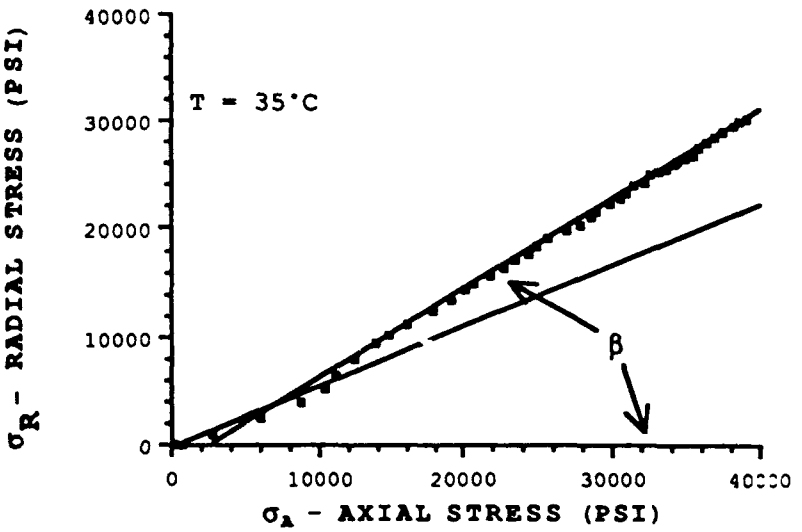

NOTE: Straight lines have been drawn through the elastic (initial) and yield parts of the leading curve as discussed in the text

Figure 3. Radial stress versus axial stress for TNT for the high strain rate conditions

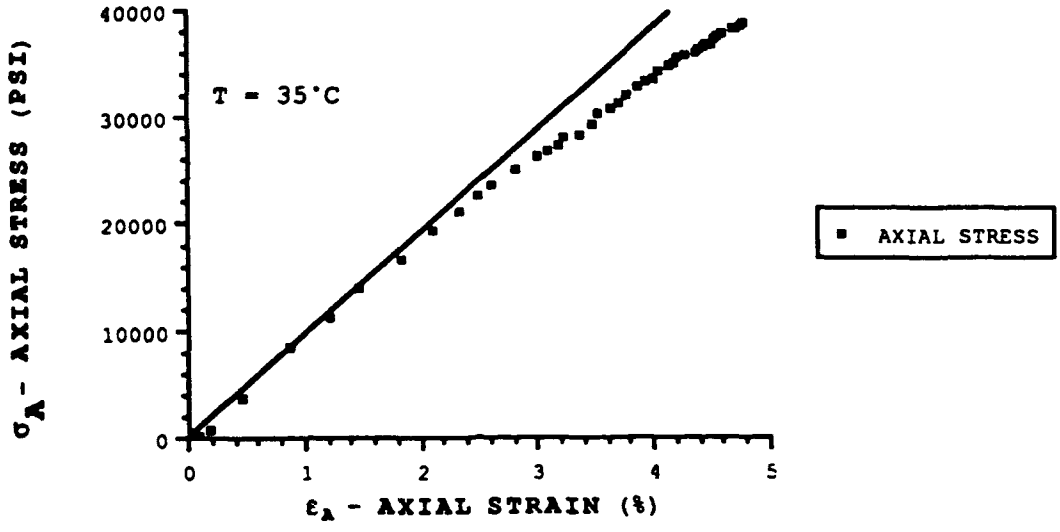

NOTE: A straight line has been drawn through the elastic (initial) part of the loading curve as discussed in the text.

Figure 4. Axial stress versus axial strain for Comp B for the high strain rate conditions

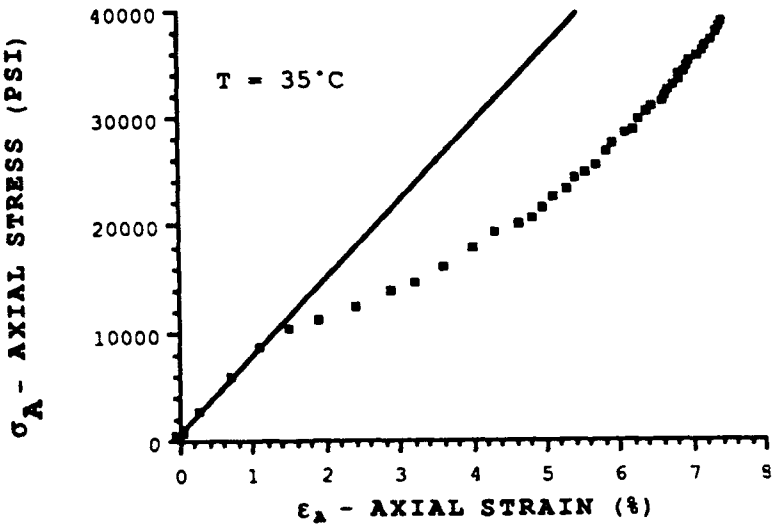

NOTE: A straight line has been drawn through the elastic (initial) part of the loading curve as discussed in the text.

Figure 5. Axial stress versus axial strain for TNT for the high strain rate conditions

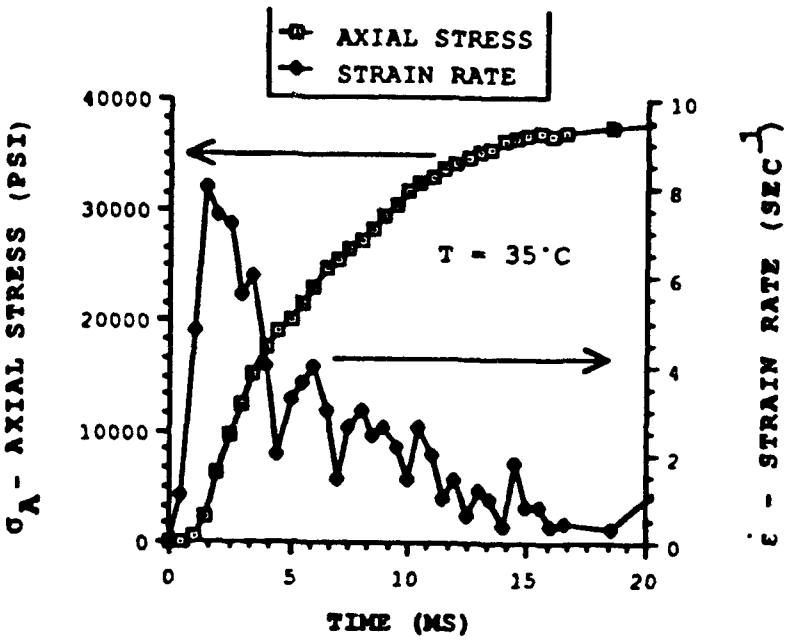

Figure 6. Typical axial stress and axial strain rate versus time for Comp B for the high strain (load) rate conditions

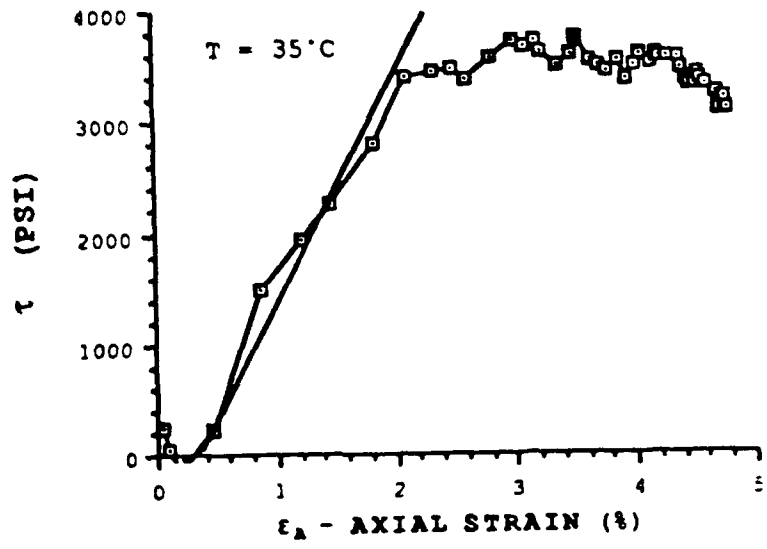

NOTE: Data has been corrected for friction (refs 2 and 20).

Figure 7. Maximum shear stress versus axial strain for Comp B for the high strain rate conditions

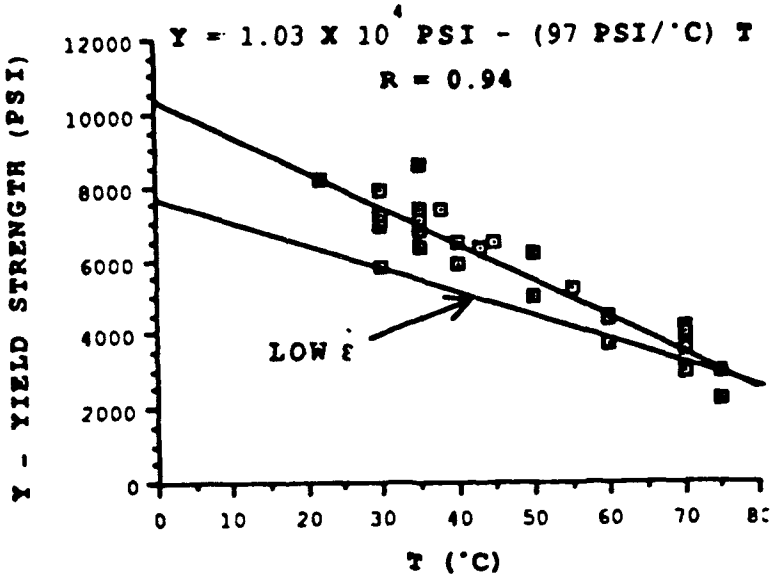

NOTE: The line through the data points is a least square fit of a straight line to the data points; R is the correlation coefficient (ref 22). Also shown is the least square straight line for the low strain rate conditions from figure 6.

Figure 8. Yield strength versus temperature for Comp B for the high strain rate conditions

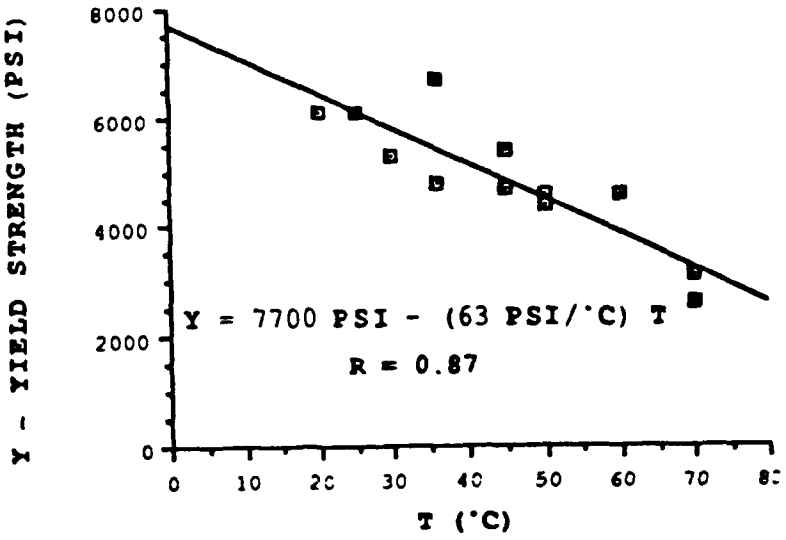

NOTE: The line is a least square fit of a straight line to the data points; R is the correlation coefficient (ref 22).

Figure 9. Yield strength versus temperature for Comp B for the low strain rate conditions

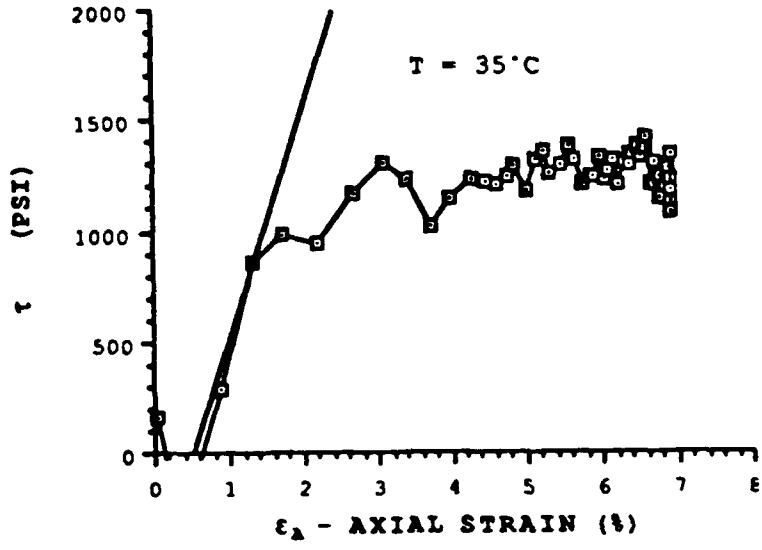

NOTE: The data have been corrected for friction (ref 2 and 20).

Figure 10. Maximum shear stress versus axial strain for TNT for the high strain rate conditions

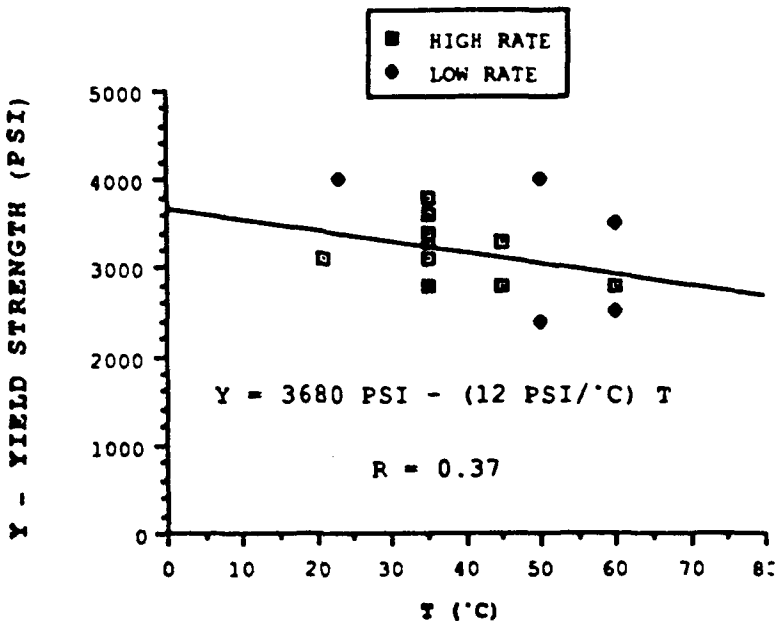

NOTE: The line is a least square fit of a straight line to the data points for the high rate conditions; R is the correlation coefficient (ref 22).

Figure 11. Yield strength versus temperature for TNT for both the low and high strain rate conditions

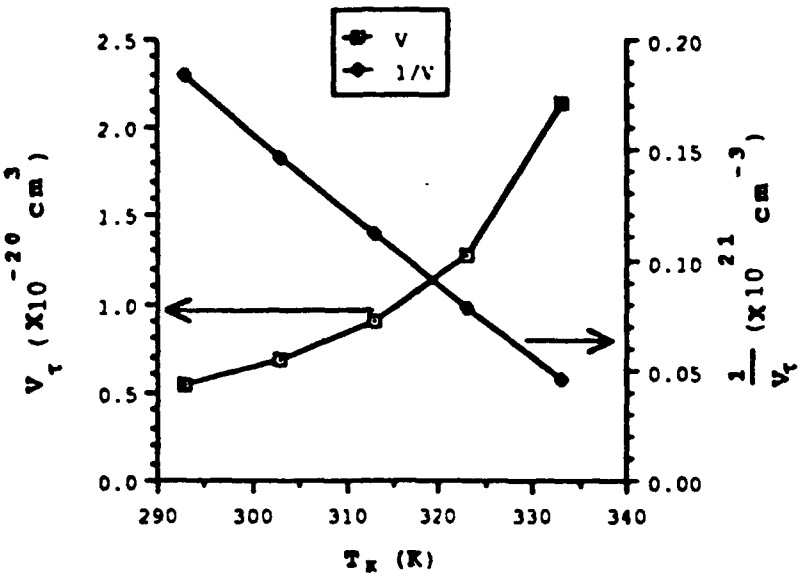

NOTE: $1/V_\tau$ is also given versus temperature.

Figure 12. Apparent activation volume, V_τ, versus temperature calculated from the experimental results of figures 6 and 7

REFERENCES

1. Pinto, J., Wiegand, D.A., and Nicolaides, S., "The Mechanical Response of TNT and a Composite, Composition B, of TNT and RDX to Compressive Stress: I. Uniaxial Stress and Fracture," Journal of Energetic Materials, 9, V9, 1991.

2. Pinto, J., Nicolaides, S., and Wiegand, D.A., "Dynamic and Quasi: Static Mechanical Properties of Comp B and TNT," Technical Report ARAED-TR-85004, ARDC, Dover, NJ, 1985.

3. Wiegand, D.A. and Pinto, J., "The Mechanical Response of TNT and a Composite, Composition B, of TNT and RDX to Compressive Stress: IV. Elastic Properties and Relaxation," Journal of Energetic Materials, 9, V9, 1991.

4. Boyle, V., Frey, R., and Blake, O., Ninth Symposium (International) on Detonation, Portland, Oregon, 1989.

5. Chaudhri, M.M., Ninth Symposium (International) on Detonation, Portland, Oregon, 1989.

6. Bourne, N.K. and Field, J.E., Ninth Symposium (International) on Detonation, Portland, Oregon, 1989.

7. Coffee, C.S., Eighth Symposium (International) on Detonation, Albuquerque, New Mexico, 1985.

8. Fishburn, B.D., "Ignition of Explosive Fills by Setback Acceleration Forces During Launch," Technical Report ARLCD-TR-85010, ARDC, Dover, New Jersey, 1985.

9. Serata, S., Bull. Mineral Industries Experimental Station, Proceedings of the Fourth Symposium on Rock Mechanics, No. 76, p 73, 1961, Pennsylvania State College.

10. Clark, N. and Schmitt, F., Engineering Science Division Information Report 558, Picatinny Arsenal, Dover, New Jersey, 1972.

11. Clark, N. and Schmitt, F., "High Strain Rate Mechanical Properties of Explosives."

12. Starkenberg, J.J., McFadden, D.L., and Lyman, O.R., Technical Report BRL-TR-2714, Ballistic Research Laboratory, Aberdeen Proving Grounds, Maryland, 1986.

13. Belanger, C., Ninth Symposium (International) on Detonation, Portland, Oregon, 1989.

14. Schaefer, S., DEA 1218 Meeting, Test Center, Meppen, FRG, June 1986.

15. Costantino, M. and Ornellas, Donald, "Initial Results for the Failure Strength of a LOVA Gun Propellant at High Pressures and Various Strain Rates," LLNL, UCRL 92441, 1985.

16. Costantino, M. and Ornellas, Donald, "The High Pressure Failure Curve for JA2," LLNL, UCRL 95555, 1987.

17. Murphy, G., "Advanced Mechanics of Materials," McGraw-Hil, New York, pp 70-85, 1946.

18. Seely, F.B. and Smith, J.O., "Advanced Mechanics of Materials," 2nd Edition, John Wiley & Sons, New York, pp 76-88, 1959.

19. Johnson, W. and Mellor, P.B., "Engineering Plasticity," John Wiley & Sons, New York, pp 62-63, 1983.

20. Wiegand, D.A., Rupel, A., and Pinto, J. , "The Mechanical Response of TNT and a Composite, Composition B, of TNT and RDX to Compressive Stress: V. Triaxial Stress, Work Hardening, and Sample to Cylinder Friction," J. Energetic Materials, 9, V9, 1991.

21. Costain, T. and Motto, R., "The Sensitivity, Perrformance, and Material Properties of Some High Explosive Formulations," Technical Report 4587, Picatinny Arsenal, New Jersey, 1973.

22. Papoulis, A., "Probability, Random Variables and Stochastic Processes," 2nd Edition, McGraw-Hill, New York, p 150, 1984.

23. Wiegand, D.A. and Pinto, J., "The Mechanical Response of TNT and a Composite, Composition B, of TNT and RDX to Compressive Stress: III. Dependence on Processing and Composition," J. Energetic Materials, 9, 349, 1991.

Wiegand, D. A. and Pinto, J. , "Fracture and Yield Strengths of Composition B and TNT as a Function of Processing Conditions and Composition," Technical Report ARAED-TR-91022, ARDEC, Picatinny Arsenal, NJ, Dec 1991

24. Perrzyna, P., "Temperature and Rate Dependent Theory of Plasticity of Crystalline Solids," Revue Phys Appl, 23, 445, 1988.

25. Li, J.C., "Dislocation Dynamics," S.R. Rosenfield, G.T. Hahn, A.L. Bement, Jr, and R.I. Jaffee, eds, McGraw-Hill, New York, p 87, 1968.

26. Seeger, A., "The Generation of Lattice Defects by Moving Dislocations and Its Application to the Temperature Dependence of the Flow-Stress of F.C.C. Crystals," Phil Mag, 40, 1194, 1955.

27. Seeger, A., "Handbuch der Physik," VII/2, S. Flugge, ed, Springer, 1958.

28. Kocks, U.F. Argon, A.S., and Ashby, M.F., "Thermodynamics and Kinetics of Slip," Pergamon Press, New York, p 131, 1975.

29. Campbell, J.D. and Ferguson, W.G., "The Temperature and Strain-Rate Dependence of the Shear Strength of Mild Steel," Phil Mag, 21, 63, 1970.

30. Rosenfield, A.R. and Hahn, G.T., "Numerical Description of the Ambient Low-Temperature and High-Strain Rate Flow and Fracture Behavior of Plain Carbon Steel," Trans Am Soc Metals, 59, 962, 1966.

31. Lanzerotti, Pinto, J., and Wolfe, A., "Broad Bandwidth Study of the Topography of the Fracture Surfaces of Explosives," Ninth Symposium (International) on Detonation, Portland, Oregon, Vol I, p 918,1989, (for example).

32. AMC Pamphlet 706-177, Engineering Design Handbook, Explosive Series, Properties of Explosives of Military, p 72, March 1966.

33. Kelly, A. and Fine, M.E., Acta Met 5, 365, 1957.

34. Brown, L.M. and Ham, E.K., Strengthening Methods in Crystals, A. Kelly and R.B. Nichiolson eds, Applied Science Publishers, England, p 39, 1971.

35. Ibid. p 75.

36. Wiegand, D.A. and Pinto, J., "Dislocation Motion in Composition B and TNT."

37. "Strengthening Methods in Crystals," A. Kelly and R.B. Nicholson, eds, Applied Science Publishers, Ltd, London, 1971.

38. Chen, H.S., Gilman, J.J., and Head, A.K., "Dislocation Multipoles and Their Role in Strain Hardening," Journal Applied Physics, 35, 2502, 1964.

39. Conrad, H., "High Strength Materials," V.F. Zackay, ed, John Wiley & Sons, New York, 1965.

40. Miura, S., Mishima, Y., and Suzuki, T., "The CRSS for Cube Slip in Ni_3 (Al,x) Single Crystals at Elevated Temperatures," Zeitschrift fur Metallukunde, 80, 157, 1989.

41. Honeycomb, R., "Plastic Deformation of Metals," Edward Arnold, Ltd., London, p 176, 1984.

42. Khristenko, N. Nauk, Izvestiya Akademii, "Influence of Strain Rate on the Variation of Flow-Stress," SSSR, Metally (Russian Metallurgy), No. 2, p 164, 1984.

DISTRIBUTION LIST

Commander
Armament Research, Development and Engineering Center
U.S. Army Armament, Munitions and Chemical Command
ATTN: SMCAR-IMI-I (5)
SMCAR-AEE-WW, D.A. Wiegand (25)
J. Pinto
B. Fishburn
M. Mezger
Y. Lanzerotti
SMCAR-AEE-W, M. Kirshenbaum
N. Slagg
SMCAR-AES, S. Kaplowitz
SMCAR-AEE, J. Lannon
SMCAR-AEE-B, D. Downs
SMCAR-AEE-BP, S.B. Bernstein
SMCAR-AEE-BR, E. Costa
SMCAR-CCH-V, F. Hildebrant
SMCAR-AEE-BR, T. Beardell
SMCAR-AET-M, A. Rupel
S. Cytron
Picatinny Arsenal, NJ 07806-5000

Commander
U.S. Army Armament, Munitions and Chemical Command
ATTN: AMSMC-GCL (D)
AMSMC-QAR-R, L. Manole
E. Bixon
AMSMC-PBM, A. E. Siklosi
D. Fair
Picatinny Arsenal, NJ 07806-5000

Administrator
Defense Technical Information Center
ATTN: Accessions Division (2)
Cameron Station
Alexandria, VA 22304-6145

Director
U.S. Army Material Systems Analysis Activity
ATTN: AMXSY-MP
AMXSY-D
Aberdeen Proving Ground, MD 21005-5066

Commander
Chemical Research, Development and Engineering Center
U.S. Army Armament, Munitions and Chemical Command
ATTN: SMCCR-MSI
Aberdeen Proving Ground, MD 21010-5423

Commander
Chemical Research, Development and Engineering Center
U.S. Army Armament, Munitions and Chemical Command
ATTN: SMCCR-RSP-A
Aberdeen Proving Ground, MD 21010-5423

Director
Ballistic Research Laboratory
ATTN: AMXBR-OD-ST
AMXBR-BLT, R. Frey
AMXBR-BLC, J. Starkenberg
AMXBR-BLT, P. Howe
AMXBR-TBT, R. Lieb
H. Rochehio
Aberdeen Proving Ground, MD 21005-5066

Chief
Benet Weapons Laboratory, CCAC
Armament Research, Development and Engineering Center
U.S. Army Armament, Munitions and Chemical Command
ATTN: SMCAR-CCB-TL
SMCAR-LCB-RA, J. Vasilakis
Watervliet, NY 12189-5000

Director
U.S. Army TRADOC Systems Analysis Activity
ATTN: ATAA-SL
White Sands Missile Range, NM 88002

Office of the Secretary of Defense
OUSD(A)
Director, Live Fire Testing
ATTN: James F. O'Bryon
Washington, DC 20301-3110

Director
U.S. Army Aviation Research and Technology Activity
Ames Research Center
Moffett Field, CA 94035-1099

Commander
U.S. Army Missile Command
ATTN: AMSMI-RD-CS-R (DOC)
Redstone Arsenal, AL 35898-5010

HQDA (SARD-TR)
Washington, DC 20310-0001

Commander
U.S. Army Tank-Automotive Command
ATTN: AMSTA-TSL, Technical Library
Warren, MI 48397-5000

Commander
U.S. Army Materiel Command
ATTN: AMCDRA-ST
5001 Eisenhower Avenue
Alexandria, VA 22333-0001

Commander
U.S. Army Laboratory Command
ATTN: AMSLC-DL
Adelphi, MD 20783-1145

Commandant
U.S. Army Infantry School
ATTN: ATSH-CD-CSO-OR
Fort Benning, GA 31905-5066

Air Force Armament Laboratory
ATTN: AFATL/DLODL
Eglin Air Force Base, FL 32542-5000

Commander
U.S. Rock Island Arsenal
ATTN: SMCAR-TL, Technical Library
AMSMC-ESM(R), W. D. Fortune
AMSMC-IRD, G. H. Cowan
Rock Island, IL 61299-5000

Commander
U.S. Army Aviation Systems Command
ATTN: AMSAV-DACL
4300 Goodfellow Blvd
St. Louis, MO 63120-1798

Commander
U.S. Army Research Office
ATTN: Chemistry Division
P.O. Box 12211
Research Triangle Park, NC 27709-2211

Commander
Naval Surface Warfare Center
ATTN: R10C, L. Roslund
R10B, M. Stosz
Silver Spring, MD 20902-5000

Commander
Naval Surface Warfare Center
ATTN: R13, J. Short
R. Bernecker
J. Forbes
Silver Spring, MD 20902-5000

Commander
Naval Weapons Center
ATTN: L. Smith
A. Amster
R. Reed, Jr.
China Lake, CA 93555

Commander
Ballistic Missile Defense Advanced Technology Center
ATTN: D. Sayles
P.O. Box 1500
Huntsville, AL 35807

Air Force Rocket Propulsion Laboratory
ATTN: AFRPL-MKPA
Edwards Air Force Base, CA 93523

Air Force Armament Technology Laboratory
ATTN: AFATL/DOIL
AFAT/DLODL
Eglin Air Force Base, FL 32542-5438

Southwest Research Institute
ATTN: M. Cowperthwaite
H. J. Gryting
6220 Culebra Road
Postal Drawer 28510
San Antonio, TX 78284

New Mexico Institute of Mining and Technology
ATTN: TERA, T. Joyner
Campus Station
Socorro, NM 87801

Director
Lawrence Livermore National Laboratory
ATTN: R. McGuire
K. Scribner
E. Lee
M.S. Costantino, L-324
M. Finger
Livermore, CA 94550

Director
Los Alamos National Laboratory
ATTN: J960, J. Ramsay
P.O. Box 1663
Los Alamos, NM 87545

Director
Sandia National Laboratory
ATTN: J. Kennedy
Albuquerque, NM 87115

Honeywell, Inc.
ATTN: R. Tompkins
10400 Yellow Circle Drive
MN 38-3300
Minnetonka, MN 55343

Johns Hopkins University
Applied Physics Laboratory
Chemical Propulsion Information Agency
ATTN: John Hannum
Johns Hopkins Road
Laurel, MD 20707

Morton Thiokol, Inc.
Louisiana Division
ATTN: Lee C. Estabrook
P.O. Box 30058
Shreveport, LA 71130

Commander
Naval Weapons Station
ATTN: L. Rothstein, Code 50 - NEDED
Yorkstown, VA 23491

John Dienes
Los Alamos National Laboratory
ATTN: MS B221
MS P952
Los Alamos, NM 87545